Energy materials

A novel scalable thinning route to enhance long-term stability of layered cathode materials for Li-ion batteries

Semih Engün[1,2], Kamil Burak Dermenci[1], Umut Savacı[1], and Servet Turan[1,*] (ID)

[1] Department of Materials Science and Engineering, Eskisehir Technical University, 26555 Eskisehir, Turkey
[2] Department of Metallurgical and Materials Engineering, Zonguldak Bulent Ecevit University, 67100 Zonguldak, Turkey

ABSTRACT

A high-pressure micro-fluidization method is applied to layered cathode materials to obtain few-layered nanosheets for the first time. The effect of the micro-fluidization on $Li(Ni_{0.333}Mn_{0.333}Co_{0.333})$ (NMC) and $LiCoO_2$ is investigated regarding crystal structure, morphology, and electrochemical properties. Micro-fluidization facilitated the exfoliation of $LiCoO_2$ layers thanks to the high shear force. As a result, the exfoliated $LiCoO_2$ nanosheets exhibited preferred orientations with more intense (003) facets. In addition, the oxygen position in the CoO_6 octahedra altered, resulting in a shortened Co–O bond length after micro-fluidization. Research demonstrates that micro-fluidized NMC and $LiCoO_2$ exhibited superior cyclic performance compared to the pristine one. Notably, it was found that micro-fluidized $LiCoO_2$ exhibited an improvement in capacity retention (75%) compared to pristine $LiCoO_2$ (21%) after 100 cycles at 0.1C. The enhanced cyclic performance of micro-fluidized NMC and $LiCoO_2$ is attributed to the surface stabilization due to the surface reconstruction of thin plates after micro-fluidization.

Introduction

Layered structured materials with a chemical formula of $LiMO_2$ where M is a transition metal like Ni, Co, and Mn are the most promising candidates among the cathode active materials for lithium-ion batteries [1]. The crystal model of $LiMO_2$ is similar to the α-$NaFeO_2$ structure with trigonal symmetry (space group: $R\overline{3}m$), where sodium and iron cations occupy different crystallographic octahedral sites within the cubic close-packed oxide array. The resulting rhombohedral structure has alternating NaO_2 and FeO_2 layers perpendicular to the [111] rock-salt plane in the ABC–ABC-stacking scheme. In $LiMO_2$, Na ions and other possible M ions (Co^{3+}, Ni^{2+}, and Mn^{4+}) were replaced by Li^+ and Fe^{3+} ions, respectively [2, 3]. Among the layered cathode materials, lithium cobalt oxide ($LiCoO_2$) has been the

---

Handling Editor: Mark Bissett.

Address correspondence to E-mail: sturan@eskisehir.edu.tr

most commonly used positive electrode material in Li-ion batteries for many years thanks to its ease of production, high energy density, high operational voltage, and good cyclic stability [4]. Although the LiCoO$_2$'s theoretical capacity is 274 mAh g^{-1}, its practical capacity is limited to 140 mAh g^{-1} due to the oxygen evolution that starts when around half of the lithiums are de-intercalated from the Li$_{1-x}$CoO$_2$ structure ($1 - x < 0.5$). The reason for the oxygen release is the overlap between the Co$^{3+/4+}$ and the O$_2-$:2p bands at about 4.2 V [5, 6]. This fact limits the use of LiCoO$_2$ only to small devices requiring relatively low energy and power densities, such as mobile phones, cameras, and laptops. Therefore, alternative layered cathode materials were improved for high-energy–density Li-ion battery applications such as electric vehicles and grid energy storage [7]. With the introduction of Ni and Mn elements into the LiCoO$_2$ structure, layered LiNi$_x$Co$_y$Mn$_z$O$_2$ (where $x + y + z \approx 1$) (NMC) cathode materials have been developed. In the NMC structure, Ni$^{3+/4+}$ and Mn$^{3+/4+}$ bands do not overlap with the O$_2-$:2p band. Therefore, structural and chemical instability reasons such as electron density removal and oxygen release do not occur in contrast to cobalt. However, due to their low octahedral site stabilization energies, Mn and Ni have less structural instability, which results in spinel transition and associated voltage drop during cycling [8].

The development of (2D) nanosheets has taken significant attention in the field of materials science. After the invention of graphene in 2004 [9], many types of 2D nanosheets comprising different elements were discovered [10]. Furthermore, researchers have recently shown increased interest in developing 2D nanosheets for Li-ion battery applications to take advantage of their short ion diffusion distance and open charge transport path advantages for fast charge and discharge performance [11]. Particularly on the anode side, researchers improved the electrochemical stability and rate capability of graphene [12], TiS$_2$ [13], and Co$_3$O$_4$ [14]. Several attempts were also made in order to produce 2D cathode materials such as LiFePO$_4$, and improved electrochemical stability was observed [15, 16]. However, little attention has been paid to obtaining 2D nanosheets for layered cathode materials because the exfoliation of layers leads to the extraction of lithium atoms from their sites and the oxidation of transition metals to higher valence states. These problems cause layered to rock-salt transformation, which is a significant concern for layered cathode materials [17, 18]. Recently, Lin et al. suggested that the rock-salt layer could shed light on the possible advantages of functionalizing the surfaces of cathode particles [19]. Besides, Su et al. demonstrated that the rock-salt layer improves the cyclic stability of the cathode due to the prevention of reactions between the active material and liquid electrolyte [20]. Therefore, we believe that 2D layered cathode nanosheets with stable surfaces may exhibit superior cycling performance than bulk cathodes. Although stacked morphologies of the layered cathodes allow producing of them as exfoliated 2D nanosheets theoretically, this is difficult due to the robust electrostatic force between the neighboring layers. Therefore, a suitable and practical top-down methodology are still needed to develop 2D layered cathode nanosheets.

Micro-fluidization is a homogenization technique carried out by passing a fluid through the micro-channels by applying high pressure (207 MPa). It is mainly used to produce nanoparticles and nanosuspensions in pharmaceutical applications. Moreover, it has also been used for the separation and dispersion of carbon nanotubes [21], few-layer graphene [22], graphene quantum dots [23], and hexagonal boron nitride nanosheets [24]. The working principle of this technique was explained elsewhere [24]. Briefly, too-high pressure is generated via the intensifier pump. It accelerates the input powder solution fed into the interaction chamber at high velocities, around 500 m/s. The powders in the solution are exposed to very high shear stresses thanks to the microchannels. Hence, low-energy bands such as Van der Waals can be broken. The most important advantage of this technique is that while applying a high shear force to the entire fluid, the plates can be exfoliated without significantly reducing size in a preferred direction. It is possible to obtain large amounts of materials with preferred orientation because of the semi-continuous nature of the process.

In the present study, we suggest a facile way to obtain the 2D-layered cathode nanosheets with desired thickness by using a micro-fluidization technique for the first time. To this end, we have studied the effect of micro-fluidization on the crystal structure and electrochemical performance. Finally, we correlated the electrochemical measurements via combined X-ray diffraction (XRD), Raman Spectroscopy, and electron microscopy techniques.

Experimental study

Pristine $Li(Ni_{0.333}Mn_{0.333}Co_{0.333})O_2$ (NMC) (Ecopro) and $LiCoO_2$ (MTI) were used for the micro-fluidization process. Firstly, 1 g cathode powder was sieved through a 63 μm sieve, and 400 mL 2-propanol was added to form a suspension before use. The resulting suspension was mixed using sonication (Sonics, 750 Vef) for one hour. Next, Sonicated $LiCoO_2$ suspension was fed into the high-pressure commercially available micro-fluidizer (Microfluidics Corp.) with 207 MPa constant intensifier pump pressure. After that, the resulting suspension was heated up to 80 °C for 12 h to obtain a dried $LiCoO_2$ powder. The crystallographic structures of all micro-fluidized cathodes were analyzed by the XRD (Rigaku Miniflex 600, Cu-Kα radiation (1.5406 Å), 2θ range of 15°–80°, 0.02 step size and 1°/min scan speed). Rietveld analysis was performed to determine the lattice parameters of cathodes using MAUD software [25]. The morphology of cathode particles was observed using scanning electron microscopy (SEM, Zeiss Supra 50 VP). The thickness of layers was monitored using a transmission electron microscope (TEM, JEOL JEM 2100F). Raman spectroscopy (WITec alpha 300) was carried out on pristine and micro-fluidized samples under 5 mW output power.

The cathode slurry was prepared by mixing 86 wt.% active material with 6 wt.% Super P (Timcal) and 6 wt.% PVdF (MTI) dissolving the mixture into N-Methyl Pyrrolidone (NMP), three times the total solid volume. The slurry prepared was spread uniformly on aluminium foil using a doctor blade (150 μm in thickness) and dried at 80 °C under a vacuum. CR2032 coin cells were fabricated in an Argon-filled glove box. Lithium foil (Alfa Aesar) was used as an anode. The electrolyte was 1 m $LiPF_6$ dissolved in ethylene carbonate and diethyl carbonate (Sigma, EC: DEC = 1:1, v/v). A Celgard 2400 PE/PP membrane separated positive and negative electrodes. The electrochemical tests were performed to analyze the charge–discharge behaviour of cathodes using the BaSyTec GmbH Test System in the 2.75–4.25 voltage range. The electrochemical impedance spectroscopy measurements were performed at 0.1 Hz–1 MHz with a 10 mV AC amplitude. All of the voltage values in this study are given against lithium oxidation potential unless stated otherwise.

Results and discussion

XRD analyses were used to see the relationship between the micro-fluidization and crystal structure of NMC and $LiCoO_2$ cathode materials. The XRD spectrums and Rietveld refinements of the pristine and micro-fluidized samples are shown in Fig. 1. Each diffraction pattern is normalized by the intensity of the (003) peak. All reflection peaks could be indexed as hexagonal (PDF No.: 01-075-0532) layered oxide structures. The intensity ratios of $I_{(003)}$ and $I_{(104)}$ peaks for each sample are shown in the inset. For the layered cathodes, the most intense Bragg peaks, namely (003) and (104), provide valuable information about crystalline ordering and perfection of crystallization. Kalyani et al. draw attention to the relation between the intensity of the (003) and (104) peaks and the crystalline ordering for $LiNiO_2$. While the (003) peak is diffracted from the layered rock-salt structure, the (104) peak is diffracted from the layered and cubic rock-salt structure. In other words, when the Li^+ and Ni^{2+} ions are entirely mixed, the intensity of (003) peaks completely disappear, and the electrochemical inactive $Li_2Ni_8O_{10}$ phase occurs [26, 27]. Figure 1a shows that the relative peak intensity ratios are 2.07 and 3.51 for the pristine and micro-fluidized $LiCoO_2$ samples. It is apparent that the intensity ratios of $I_{(003)}/I_{(104)}$ increase with the micro-fluidization process, which shows that the formation of nanosheets results in excellent layered morphology. The calculated peak intensity ratio of bulk $LiCoO_2$ as 2.07 seems consistent with previous research that found 2.00 [18]. However, the peak intensity ratio of micro-fluidized $LiCoO_2$ calculated as 3.51 is lower than 7.6 in the previous study. This difference may be due to the disorder induction into the $LiCoO_2$ crystal structure during the micro-fluidization process. Another possible explanation for this difference is the thickness differences between nanosheets. On the other hand, the relative peak ratios for the pristine and micro-fluidized NMC samples are calculated as 1.47 and 1.67, respectively (Fig. 1b). Although the relative peak ratio of micro-fluidized NMC is also higher than that of pristine one, it is not as higher as that of $LiCoO_2$ and is still below 2.00. This discrepancy could be attributed to the morphology of NMC powders which is explained in more detail in the SEM results. Crystal structure changes, such as lattice parameters and oxygen positions, were quantified using the Rietveld refinement with $LiCoO_2$ and
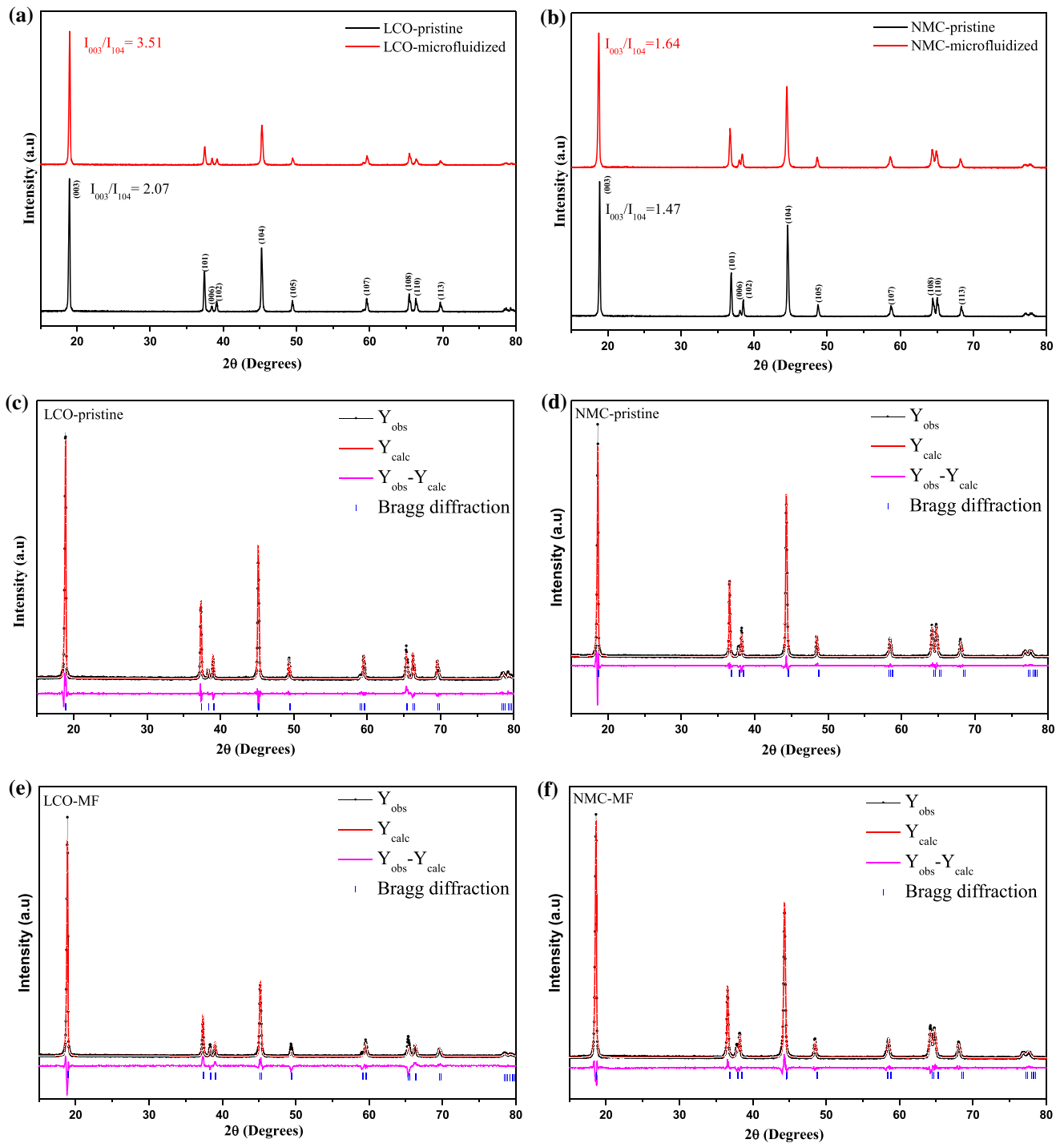
Figure 1 XRD patterns of pristine and micro-fluidized **a** $LiCoO_2$ and **b** NMC; refined spectrums of pristine **c** $LiCoO_2$, and **d** NMC and micro-fluidized **e** $LiCoO_2$ and **f** NMC.

$LiNi_{0.333}Mn_{0.333}Co_{0.333}$ phase models (Fig. 1c–f). The results were summarized with weighted (R_{wp}), expected (R_{exp}) profiles, and the goodness of fit ($\chi^2 = R_{wp}/R_{exp}$) in Table 1.

It can be seen from Table 1 that the lattice parameters 'a' and 'c' define the size of the hexagonal lattice. In the case of the NMC particles, the 'c' lattice parameter decreased by micro-fluidization. It seems possible that this reduction is due to induced

disorder during the micro-fluidization process [28]. However, the enlargement of the 'c' lattice parameter was observed with micro-fluidization at the LiCoO$_2$ side. This finding shows that the LiCoO$_2$ layers were exfoliated due to the high-shear force effect of the micro-fluidization process [18]. Further data from Table 1 shows that the 'c/a' ratio for all samples is around 4.9 indicating an ideal cubic-close packed oxygen lattice [29]. The refined 'z' parameters showing the oxygen position and are responsible for the deformation of the oxygen octahedron surrounding TM cations [30] are also given in Table 1.

Figure 2 shows the calculated Co–O bond distance and O–Co–O bond angle of the pristine, micro-fluidized, and theoretical LiCoO$_2$ model according to the 'z' parameter. The pristine sample has a lower Co–O bond distance and a higher O–Co–O bond angle (parallel to the *c*-direction) than the theoretical model. This result suggests that the pristine Li$_x$CoO$_2$ sample has less lithium than the nominal amount. Thus, the Co–O bond distance decreased, and the O–Co–O bond angle increased by decreasing 'x' [34]. Furthermore, the micro-fluidized LiCoO$_2$ has the shortest Co–O bond distance and higher O–Co–O bond angle (parallel to the *c*-direction). It seems possible that this result is due to the partial extraction of Li ions during the exfoliation resulting in spin ordering of the Co ions [31].

The Raman spectroscopy was conducted further to assess the effect of micro-fluidization on the bonding structure, and results are given in Fig. 3. The Raman analysis showed two characteristic spectra belonging to the layered cathodes. While the E_g band indicates O-Co–O bending in the a–b plane at 485 cm^{-1}, the A_{1g} band shows the Co–O stretching mode along the *c*-axis at 593 cm^{-1} [32]. The broad-spectrum nature of NMC due to the different oxidation states of Ni ions is explained in detail elsewhere [33]. It is seen from Fig. 3a, b that E_g and A_{1g} bands broadened and shifted downwards from the pristine state with the micro-fluidization of NMC and LiCoO$_2$, respectively. The polyhedral distortion and motion of the oxygen atoms may result in peak shifts [34]. These results also align with the Co–O bond distance and O–Co–O bond angle measurements in Fig. 2. For the LiCoO$_2$ samples, there is also a minor peak around the

Table 1 Lattice parameters and ratios (*a*, *c* and *c/a*) and oxygen parameters (z_{oxy}) of pristine and micro-fluidized NMC and LiCoO$_2$ powders given with reliability factors of expected (R_{exp}) and weighed (R_{wp}) profiles and goodness of fit (χ^2) values

| Sample	*a* (Å)	*c* (Å)	*c/a*	Z_{oxy}	R_{exp} (%)	R_{wp} (%)	χ^2
NMC-pristine	2.877 ± 5.39E−5	14.270 ± 5.20E−4	4.962	0.242 ± 1.71E−4	9.76	14.07	1.44
NMC-MF	2.877 ± 6.44E−5	14.259 ± 6.52E−4	4.958	0.239 ± 1.60E−4	8.80	11.88	1.35
LiCoO$_2$-pristine	2.819 ± 5.61E−5	14.069 ± 5.42E−4	4.990	0.262 ± 2.39E−4	12.80	15.93	1.24
LiCoO$_2$-MF	2.819 ± 1.01E−4	14.072 ± 1.16E−3	4.990	0.270 ± 3.34E−4	12.04	21.39	1.78
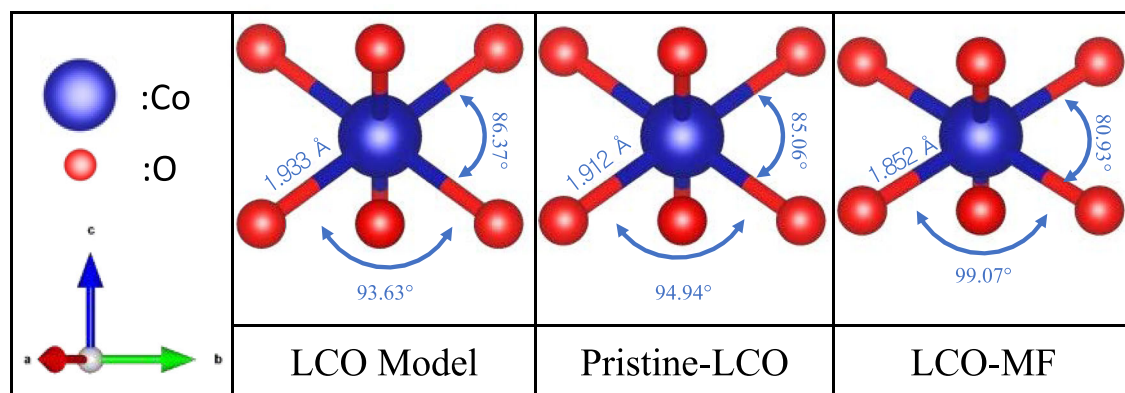
Figure 2 Comparison of Co–O bond lengths and O-Co–O bond angles of pristine and micro-fluidized LiCoO$_2$ samples based on theoretical CoO$_6$ octahedra model.

**Figure 3** Raman spectra of pristine and micro-fluidized **a** NMC **b** LiCoO$_2$ cathodes.
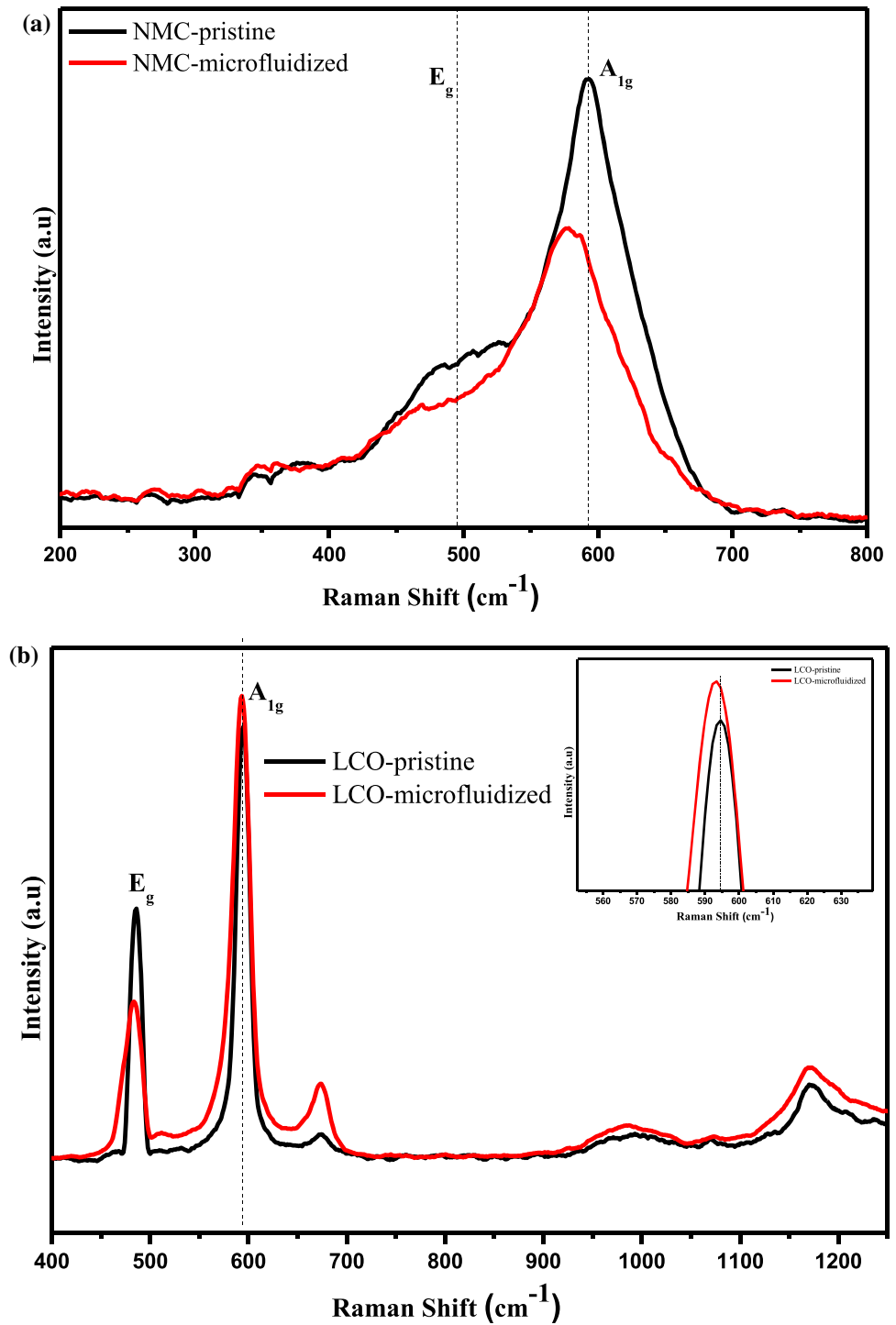
693 cm^{-1} showing the Co$_3$O$_4$ formation during the micro-fluidization process. The formation of Co$_3$O$_4$ was assigned to the LiCoO$_2$ decomposition into O$_2$ and Co$_3$O$_4$ (Eq. 3) due to the loss of more than 0.50 lithium [35–37]. However, since there is no Co$_3$O$_4$ peak detected on XRD patterns, it is believed that Co$_3$O$_4$ content is found only as a thin layer at the LiCoO$_2$ surface.

$$\text{Li}_{0.50}\text{CoO}_2 \leftrightarrow 0.50\text{LiCoO}_2 + \frac{1}{6}\text{Co}_3\text{O}_4 + \frac{1}{6}\text{O}_2 \qquad (3)$$
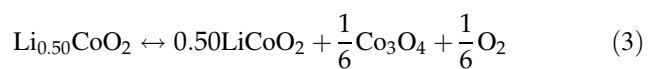
Secondary electron SEM images of pristine and micro-fluidized cathodes are shown in Fig. 4. The
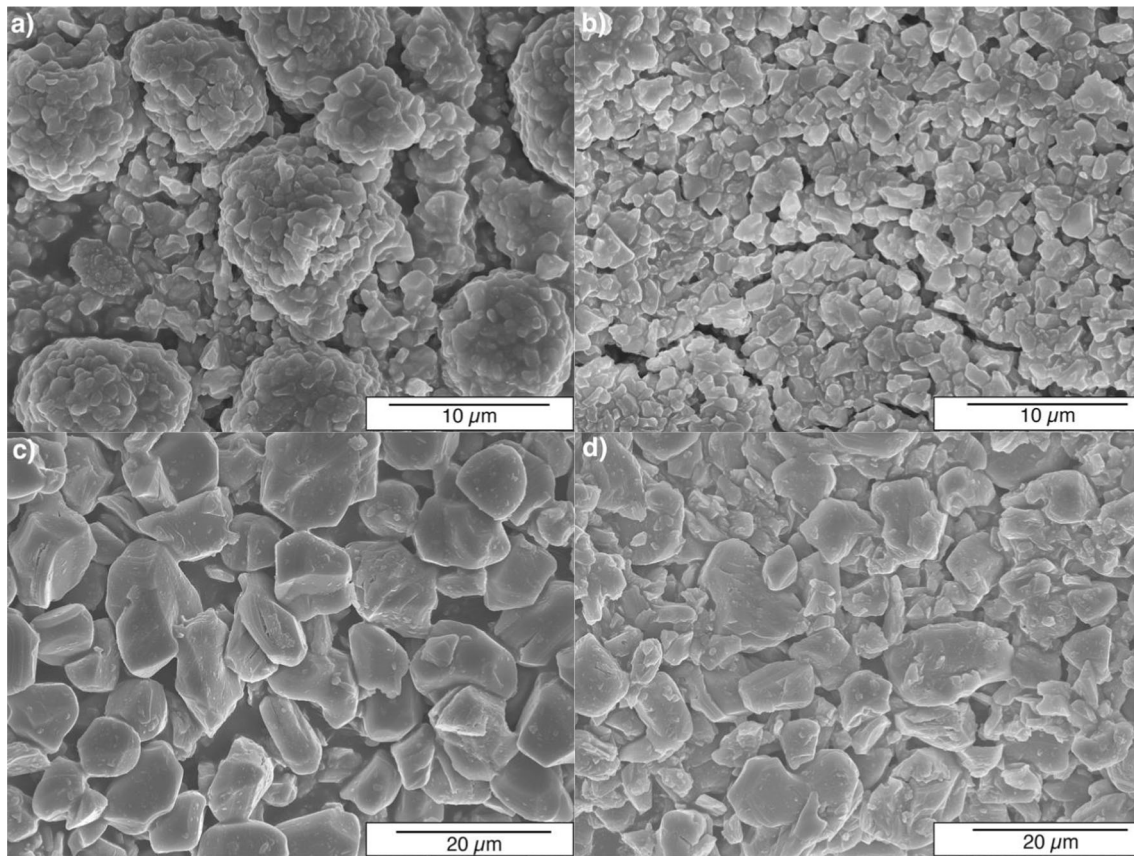
Figure 4 Secondary electron SEM images of **a** pristine NMC, **b** micro-fluidized NMC, **c** pristine LiCoO₂, **d** micro-fluidized LiCoO₂ particles.

shape of the pristine NMC has a spherical secondary particle nature, and the primary particles are closely packed without apparent gaps in between (Fig. 4a). After micro-fluidization, the secondary particles are disintegrated into the primary particles having loose contact (Fig. 4b). Pristine LiCoO₂ particles have the typical smooth bulk morphology consisting of thin layers with approximately 10 μm particle size (Fig. 4c). Moreover, it can be observed that pristine LiCoO₂ powders get thinner with micro-fluidization while preserving their characteristic stacked morphology (Fig. 4d).

We performed TEM analysis to assess the layer morphology, elemental distribution, and crystal structure of micro-fluidized LiCoO₂ cathodes. It can be seen from the bright-field TEM images that pristine LiCoO₂ powder appears as shaded due to being in bulk form (Fig. 5a). As the sample is micro-fluidized, transparent layers stand out by thinning LiCoO₂ stacks (Fig. 5b). This finding has important implications for the micro-fluidization process, which

helps to reduce the thickness of LiCoO₂ layer stacks thanks to the exfoliation effect. Additionally, EDX analyses were done from the edge toward the center of the micro-fluidized LiCoO₂ sample (labelled as 1, 2, and 3 in Fig. 5c). The corresponding spectrums are shown in Fig. 5 (d), and chemical compositions are given in Table 2. As a result, the oxygen content increases from edge to inside the sample, pointing out that the edges of LiCoO₂ get more oxygen-deficient due to the edge disordering of LiCoO₂ nanosheets [38]. These results also support the Raman spectra showing Co₃O₄ formation with micro-fluidization. HRTEM image of the micro-fluidized LiCoO₂ (Fig. 5e) confirms the edge disordering with a few atom thicknesses, which is known for its chemical resistivity against liquid electrolyte reactions [39–41]. Although the surface seems to be layered structured (space group $R\bar{3}m$), previous studies showed that a surface reconstruction with a few atom thicknesses occurs along with the (003) facets [42]. This combination of findings provides some support
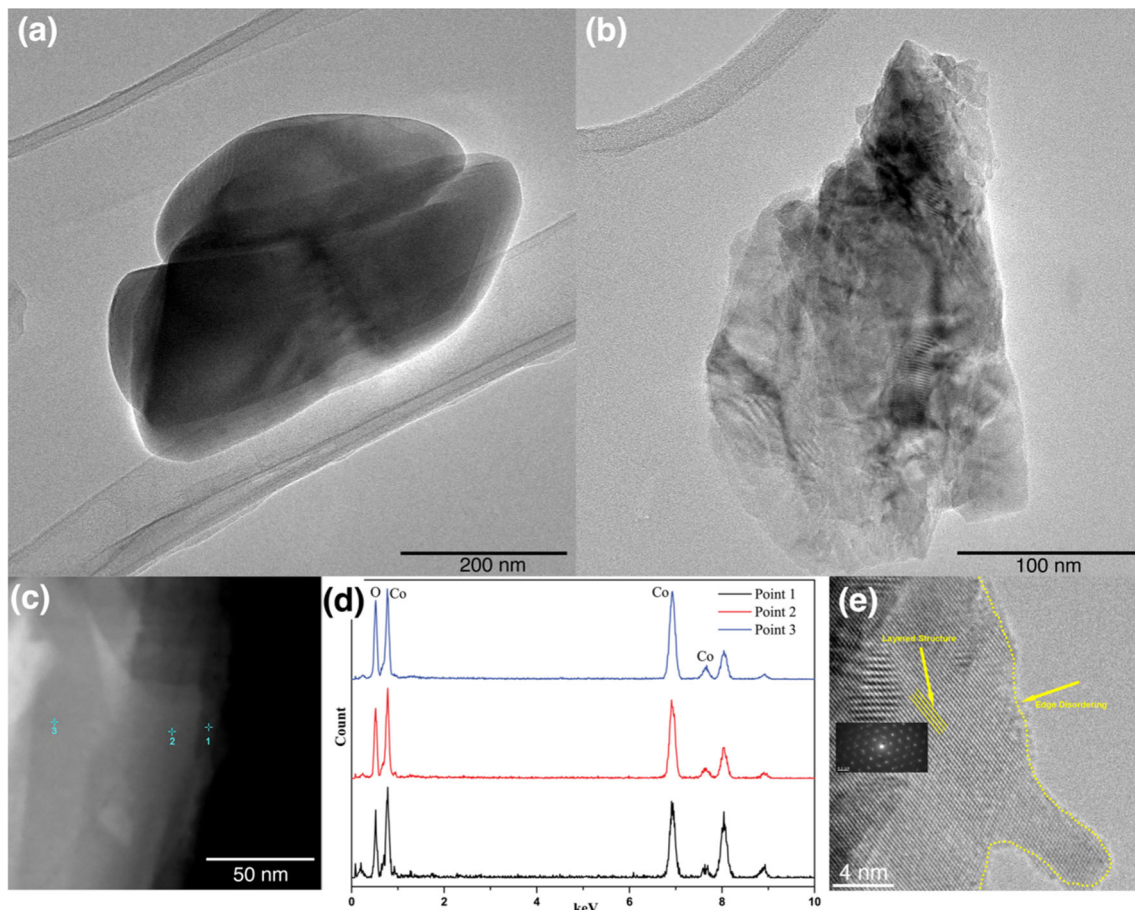
Figure 5 TEM image of **a** pristine and **b** micro-fluidized LiCoO$_2$, **c** STEM HAADF image of micro-fluidized LiCoO$_2$ (d-f) EDX spectra of positions 1–3 g) HRTEM image showing the edge of micro-fluidized LiCoO$_2$.

Table 2 Elemental distribution of positions in Fig. 4c

	O (at.%)	Co (at.%)
Point 1	64.01	35.99
Point 2	66.52	33.48
Point 3	65.92	34.08

for LiCoO$_2$ nanosheets being more stable against the liquid electrolyte reactions in all directions. However, the nanosheets compromise the battery's rate capability due to the reduced electronic and ionic conductivity [17, 43, 44].

The effect of micro-fluidization on the electrochemical performance of NMC and LiCoO$_2$ materials has been studied in a potential range between 2.75 and 4.25 V under room temperature. The initial charge/discharge capacities of the pristine and micro-fluidized NMC samples were measured at 0.1C, and results are given in Fig. 6a. The pristine NMC delivered a higher charge and discharge capacity (176 and 143 mAh g^{-1}, respectively) than the micro-fluidized NMC (161 and 128 mAh g^{-1}, respectively). The coulombic efficiency of the pristine and micro-fluidized NMC are nearly the same (81% and 80%). In the case of the LiCoO$_2$, the micro-fluidized sample delivered a higher charge capacity (164 mAh g^{-1}) than the pristine LiCoO$_2$ (155 mAh g^{-1}) (Fig. 6b). Besides, discharge capacities are nearly identical (146 mAh g^{-1} and 145 mAh g^{-1}, respectively). The decrease in coulombic efficiency (93.5% for pristine-LiCoO$_2$ and 89.0% for micro-fluidized LiCoO$_2$) shows that the reversible capacity decreases with micro-fluidization, which may be due to the crystal structure distortion.

Pristine and micro-fluidized NMC and LiCoO$_2$ cathodes were cycled for 100 cycles between 2.75 and 4.25 V at 0.1 C-rate. Figure 7 displays the cyclic performance of pristine and micro-fluidized NMC electrodes. The capacities of pristine and micro-fluidized NMC are 76 and 88 mAh g^{-1}, respectively, after the

Figure 6 First charge and discharge performances of pristine and micro-fluidized **a** NMC and **b** LiCoO$_2$ cathodes.
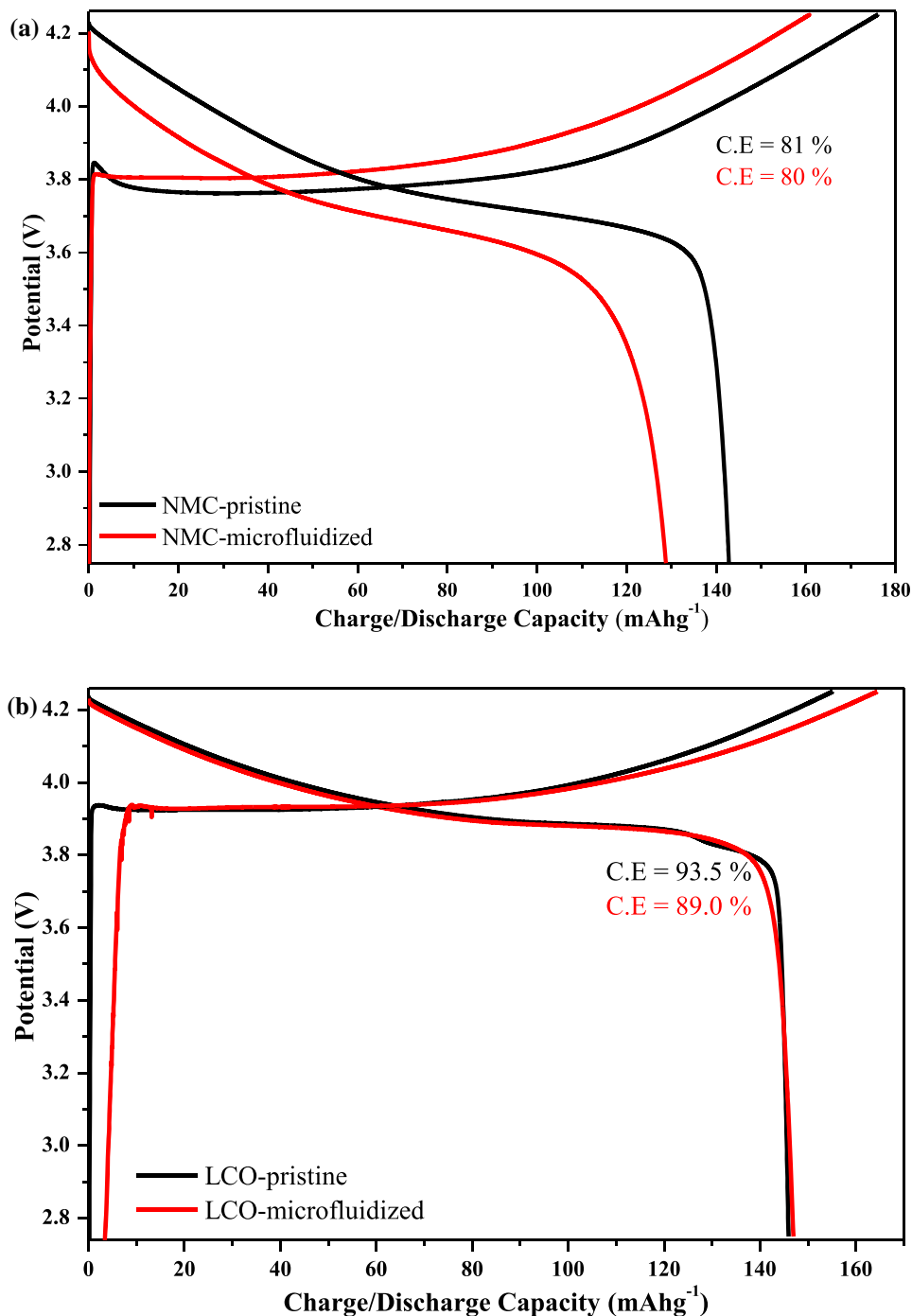
100th cycle. Even having a lower initial discharge capacity, the micro-fluidized sample retained more than 68% of its capacity after 100 cycles (Fig. 7b). This value is limited to 53% for pristine-NMC (Fig. 7a). It seems possible that the improved cyclic stability of micro-fluidized NMC is due to the surface reconstruction of disintegrated primary particles, which were shielded in secondary particles before [45, 46].
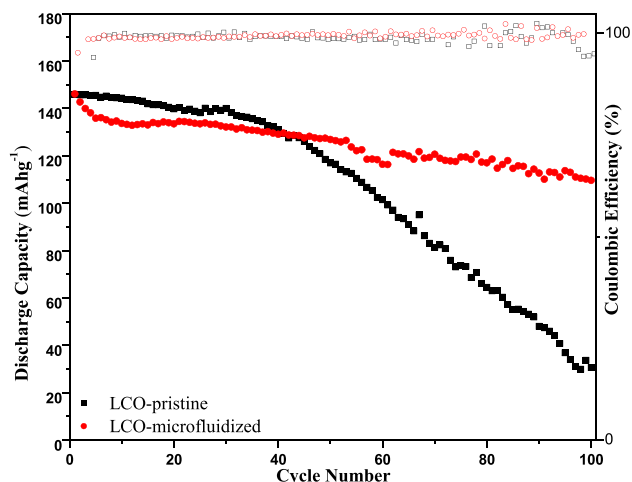
The cyclic stabilities of pristine and micro-fluidized LiCoO$_2$ samples at 0.1 C are shown in Fig. 8. Pristine LiCoO$_2$ preserved its discharge capacity of only 31 mAh g^{-1} after 100 cycles representing 21% of its initial discharge capacity (146 mAh g^{-1}). This capacity retention rate of pristine LiCoO$_2$ is similar to previous studies [47–49]. Such a high capacity fade can be attributed to mechanical failure because of the

Figure 7 Cyclic performances of **a** pristine and **b** micro-fluidized NMC cathode materials.
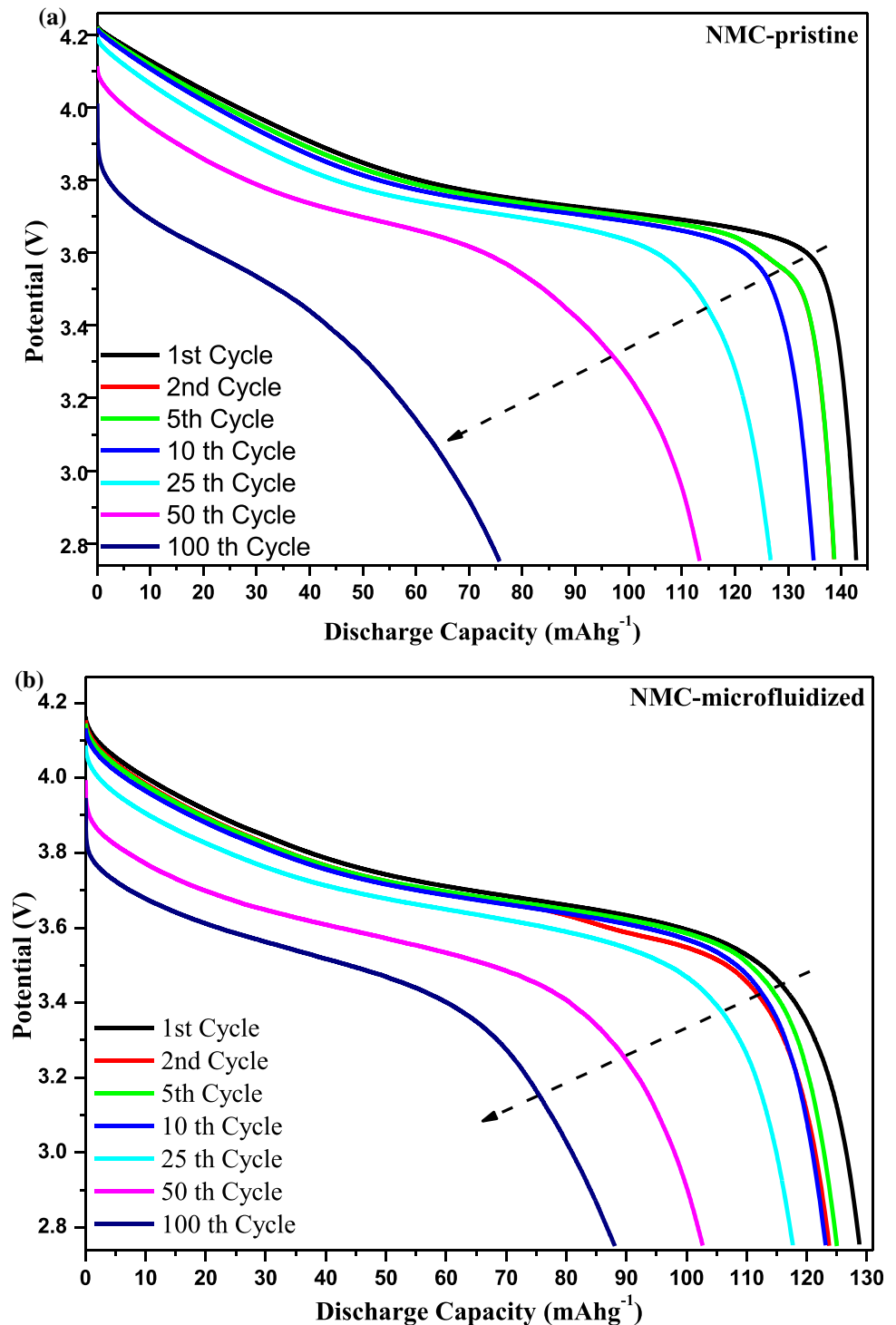
structural changes during cycling above 4.25 V [50]. Although the pristine and micro-fluidized LiCoO$_2$ have the same discharge capacity at the first cycle, the micro-fluidized sample shows faster capacity decay during the first ten cycles and then is stabilized. This rapid and irreversible capacity loss confirms the association between the surface reconstruction layer formation and the surface stabilization of exfoliated LiCoO$_2$ nanosheets [51, 52]. However, compared to the pristine LiCoO$_2$ electrode, micro-fluidized LiCoO$_2$ showed much better capacity retention than the pristine LiCoO$_2$ with 75%. Therefore, the primary

Figure 8 Cyclic performances of pristine and micro-fluidized LiCoO₂ cathode materials.

outcome of the LiCoO₂ nanosheet cathode material, as confirmed in relevant literature based on the exfoliation process [21]. The stable, protective layer nature of the disordered surface and edges of LiCoO₂ nanosheets resulted in the retention of the reaction between liquid electrolyte and active material.

Rate performances of pristine and corresponding micro-fluidized NMC and LiCoO₂ at different charge/discharge C-rates from 0.1C, 0.2 C, 0.5 C, and 1C between 2.75 to 4.25 V were also examined. Figure 9 shows the rate capabilities of pristine and micro-fluidized NMC cathodes. Micro-fluidization's clear benefit in enhancing discharge capacity at high C-rates could not be identified for the NMC cathode (Fig. 9a). This result may be explained because disintegrated primary particles with micro-fluidization have loose contact leading to longer Li-ion pathways and impedance. In the case of LiCoO₂, pristine and micro-fluidized samples exhibited almost the same discharge capacity at a 0.1C rate (Fig. 8b). However, the difference between the discharge capacities of the two samples increased with higher C rates. The decreased rate capability of micro-fluidized LiCoO₂ may be attributed to the worsened Li-ion conductivity of particles due to the surface rock-salt layer, according to recent studies [44].

We conducted electrochemical impedance spectroscopy (EIS) at room temperature under the same conditions to analyze the micro-fluidization effect on charge transfer kinetics. The Nyquist plots of pristine

and micro-fluidized electrodes are presented in Fig. 10. The spectra included a high-frequency semi-circle associated with the ohmic resistance (R_s), medium frequency semi-circle related to the solid-electrolyte interface and charge transfer (R_{ct}), and a low-frequency tail was a clue of Warburg-type lithium-ion migration. We calculated the R_s and R_{ct} values from Nyquist curves fitting with corresponding equivalent circuit models presented as an inlet in Fig. 10 and gave results in Table 3. Notably, the charge transfer resistance of pristine NMC (Fig. 10a) and LiCoO₂ (Fig. 10b) was decreased due to the micro-fluidization process. This increase in the R_{ct} value was attributed to the evolution of a resistive layer that impedes ionic transport due to the surface reconstruction of micro-fluidized samples [53].

Conclusion

This study aimed to exfoliate NMC and LiCoO₂ cathode particles using a novel micro-fluidization technique inspired by 2D materials such as graphene. The results show that the micro-fluidized cathode samples have better cyclic stability than that pristine samples. Notably, LiCoO₂ showed superior capacity retention with 78% after 100 cycles. The exfoliated cathode layers having more (003) facets are more stable against the liquid electrolyte reactions due to the surface reconstruction (Co₃O₄ formation), confirmed by XRD, Raman, and TEM analysis. The study's primary limitation is reducing rate capability due to the looser contact of particles with fragmentation and surface reconstruction after exfoliation with the micro-fluidization process. The electrochemical impedance spectroscopy results show increasing charge transfer resistance with micro-fluidization correlated with this limitation of both layered cathodes.

Notwithstanding these limitations, this study offers valuable insight into exfoliated layered cathodes for long-lasting lithium-ion batteries. A greater focus on reproducing secondary particles with controlled shape and heat treatment could produce interesting findings that account for more enhanced rate capability.

Figure 9 Rate capabilities of pristine and micro-fluidized **a** NMC and **b** LiCoO₂ cathode materials.
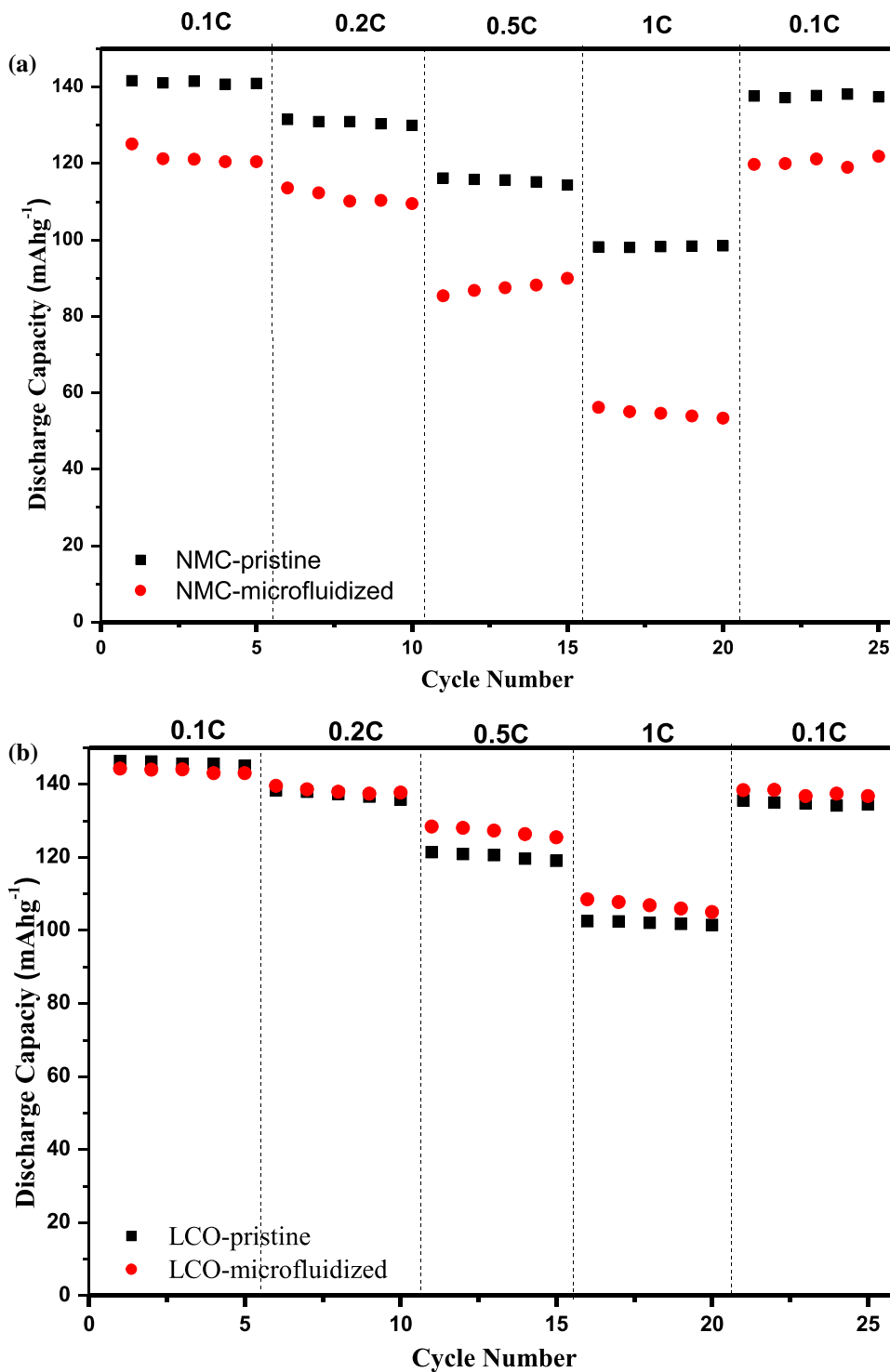
Figure 10 The Nyquist plots of pristine and micro-fluidized **a** NMC and **b** LiCoO$_2$ cathode materials.
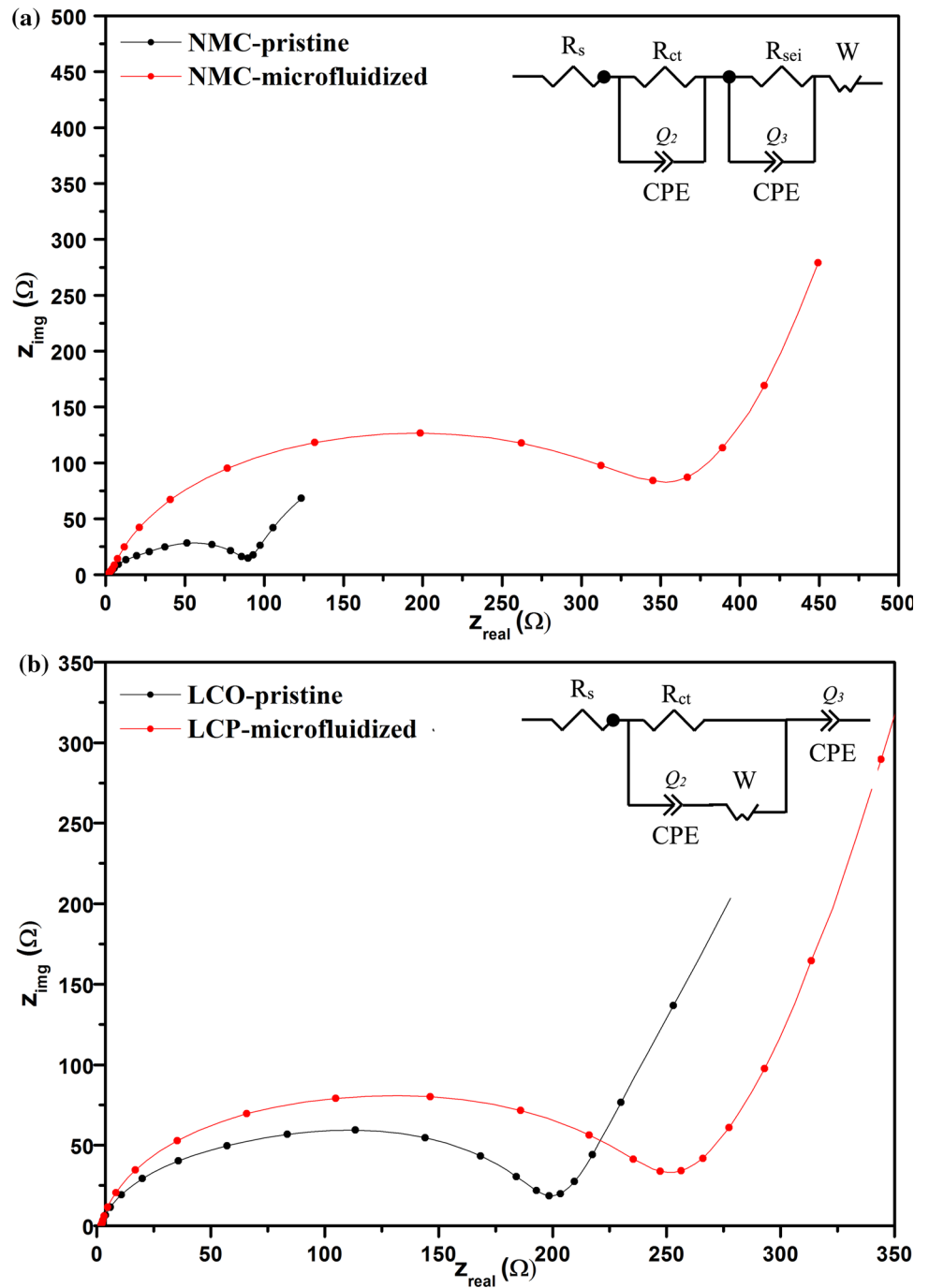
Table 3 Ohmic transfer and charge transfer values of pristine and micro-fluidized cathodes

Sample	R_s (Ω)	R_{ct} (Ω)	χ^2
NMC-pristine	1.64	80.31	4.39×10^{-3}
NMC-micro-fluidized	1.38	326	7.32×10^{-3}
LiCoO$_2$-pristine	1.63	182	4.23×10^{-3}
LiCoO$_2$-micro-fluidized	1.77	228	2.42×10^{-3}

Acknowledgements

Declarations

Conflict of interests The authors declare that they have no known competing financial interests or personal relationships that could have appeared to influence the work reported in this paper.

References

[1] Nitta N, Wu F, Lee JT, Yushin G (2015) Li-ion battery materials: present and future. Mater Today 18:252–264. https://doi.org/10.1016/j.mattod.2014.10.040

[2] Delmas C, Fouassier C, Hagenmuller P (1980) Structural classification and properties of the layered oxides. Physica B+C 99:81–85. https://doi.org/10.1016/0378-4363(80)90214-4

[3] Chakraborty A, Kunnikuruvan S, Kumar S et al (2020) Layered cathode materials for lithium-ion batteries: review of computational studies on LiNi$_{1-x-y}$Co$_x$Mn$_y$O$_2$ and LiNi$_{1-x-y}$Co$_x$Al$_y$O$_2$. Chem Mater 32:915–952. https://doi.org/10.1021/acs.chemmater.9b04066

[4] Kim H, Kong M, Kim K et al (2009) Electrochemical characteristics of LiFeP$_4$/LiCoO$_2$ mixed electrode for Li secondary battery. J Electroceram 23:219–224. https://doi.org/10.1007/s10832-007-9403-0

[5] Radin MD, Hy S, Sina M et al (2017) Narrowing the gap between theoretical and practical capacities in Li-Ion layered oxide cathode materials. Adv Energy Mater 7:1602888–1602921. https://doi.org/10.1002/aenm.201602888

[6] Venkatraman S, Shin Y, Manthiram A (2003) Phase relationships and structural and chemical stabilities of charged Li$_{1-x}$CoO$_{2-\delta}$ and Li$_{1-x}$ Ni$_{0.85}$Co$_{0.15}$O$_{2-\delta}$ Cathodes. Electrochem Solid-State Lett 6:A9–A12. https://doi.org/10.1149/1.1525430

[7] Ohzuku T, Makimura Y (2001) Layered lithium insertion material of LiCo$_{1/3}$Ni$_{1/3}$Mn$_{1/3}$O$_2$ for lithium-ion batteries. Chem Lett 30:642–643

[8] Manthiram A (2020) A reflection on lithium-ion battery cathode chemistry. Nat Commun 11:1550–1559. https://doi.org/10.1038/s41467-020-15355-0

[9] Novoselov KS, Geim AK, Morozov Sv et al (2004) Electric field effect in atomically thin carbon films. Science 1979(306):666–669. https://doi.org/10.1126/science.1102896

[10] Kim NY, Blake S, De D et al (2020) Two-dimensional nanosheet-based photonic nanomedicine for combined gene and photothermal therapy. Front Pharmacol 10:1573–1587. https://doi.org/10.3389/fphar.2019.01573

[11] Xiong P, Peng L, Chen D et al (2015) Two-dimensional nanosheets based Li-ion full batteries with high rate capability and flexibility. Nano Energy 12:816–823. https://doi.org/10.1016/j.nanoen.2015.01.044

[12] Wu Z-S, Ren W, Xu L et al (2011) Doped graphene sheets as anode materials with superhigh rate and large capacity for lithium ion batteries. ACS Nano 5:5463–5471. https://doi.org/10.1021/nn2006249

[13] Liu SH, Jia HP, Han L et al (2012) Nanosheet-constructed porous TiO$_2$-B for advanced lithium ion batteries. Adv Mater 24:3201–3204. https://doi.org/10.1002/adma.201201036

[14] Wang X, Wu XL, Guo YG et al (2010) Synthesis and lithium storage properties of Co$_3$O$_4$ nanosheet-assembled multi-shelled hollow spheres. Adv Funct Mater 20:1680–1686. https://doi.org/10.1002/adfm.200902295

[15] Ren MM, Zhou Z, Gao XP et al (2008) LiVOPO4 hollow microspheres: one-pot hydrothermal synthesis with reactants as self-sacrifice templates and lithium intercalation performances. J Phys Chem C 112:13043–13046

[16] Rui X, Zhao X, Lu Z et al (2013) Olivine-type nanosheets for lithium ion battery cathodes. ACS Nano 7:5637–5646. https://doi.org/10.1021/nn4022263

[17] Yan P, Zheng J, Zheng J et al (2016) Ni and Co segregations on selective surface facets and rational design of layered lithium transition-metal oxide cathodes. Adv Energy Mater 6:1502455–1502464. https://doi.org/10.1002/aenm.201502455

[18] Tai Z, Subramaniyam CM, Chou S-L et al (2017) Few atomic layered lithium cathode materials to achieve ultrahigh rate capability in lithium-ion batteries. Adv Mater

29:1700605–1700613. https://doi.org/10.1002/adma.201700605

[19] Lin F, Markus IM, Nordlund D et al (2014) Surface reconstruction and chemical evolution of stoichiometric layered cathode materials for lithium-ion batteries. Nat Commun 5:3529–3538. https://doi.org/10.1038/ncomms4529

[20] Su Y, Yang Y, Chen L et al (2018) Improving the cycling stability of Ni-rich cathode materials by fabricating surface rock salt phase. Electrochim Acta 292:217–226. https://doi.org/10.1016/j.electacta.2018.09.158

[21] Karagiannidis PG, Hodge SA, Lombardi L et al (2017) Microfluidization of graphite and formulation of graphene-based conductive ınks. ACS Nano 11:2742–2755. https://doi.org/10.1021/acsnano.6b07735

[22] Baskut S, Cinar A, Seyhan AT, Turan S (2018) Tailoring the properties of spark plasma sintered SiAlON containing graphene nanoplatelets by using different exfoliation and size reduction techniques: Anisotropic electrical properties. J Eur Ceram Soc 38:3787–3792. https://doi.org/10.1016/j.jeurceramsoc.2018.04.066

[23] Buzaglo M, Shtein M, Regev O (2016) Graphene quantum dots produced by microfluidization. Chem Mater 28:21–24. https://doi.org/10.1021/acs.chemmater.5b03301

[24] Yurdakul H, Göncü Y, Durukan O et al (2012) Nanoscopic characterization of two-dimensional (2D) boron nitride nanosheets (BNNSs) produced by microfluidization. Ceram Int 38:2187–2193. https://doi.org/10.1016/j.ceramint.2011.10.064

[25] Lutterotti L, Bortolotti M, Ischia G et al (2007) Rietveld texture analysis from diffraction images. Zeitschrift fur Kristallographie 2007:125–130. https://doi.org/10.1524/9783486992540-020

[26] Kalyani P, Kalaiselvi N (2005) Various aspects of $LiNiO_2$ chemistry: a review. Sci Technol Adv Mater 6:689–703. https://doi.org/10.1016/j.stam.2005.06.001

[27] Morales J, Pérez-Vicente C, Tirado JL (1990) Cation distribution and chemical deintercalation of $Li_{1-x}Ni_{1+x}O_2$. Mater Res Bull 25:623–630. https://doi.org/10.1016/0025-5408(90)90028-Z

[28] Pan T, Alvarado J, Zhu J et al (2019) Structural degradation of layered cathode materials in lithium-ion batteries induced by ball milling. J Electrochem Soc 166:A1964–A1971. https://doi.org/10.1149/2.0091910jes

[29] Broussely M, Perton F, Biensan P et al (1995) $LixNiO_2$, a promising cathode for rechargeable lithium batteries. J Power Sources 54:109–114. https://doi.org/10.1016/0378-7753(94)02049-9

[30] Molenda J (2019) Cathode electronic structure impact on lithium and sodium batteries parameters. In: Lithium-ion batteries - thin film for energy materials and devices.

London, United Kingdom: IntechOpen, 2019 [Online]. https://www.intechopen.com/chapters/65700. https://doi.org/10.5772/intechopen.83606

[31] Zheng X, Chen Y, Zheng X et al (2019) Electronic structure engineering of $LiCoO_2$ toward enhanced oxygen electrocatalysis. Adv Energy Mater 9:1803482–1803492. https://doi.org/10.1002/aenm.201803482

[32] Rao MC (2010) Raman investigations on laser ablated $LiCoO_2$ and $LiTi_xCo_{1-x}O_2$ thin film cathodes. Optoelectron Adv Mater Rapid Commun 4:2088–2091

[33] Flores E, Novák P, Berg EJ (2018) In situ and Operando Raman spectroscopy of layered transition metal oxides for Li-ion battery cathodes. Front Energy Res 6:82–98. https://doi.org/10.3389/fenrg.2018.00082

[34] Wang X, Loa I, Kunc K et al (2005) Effect of pressure on the structural properties and Raman modes of $LiCoO_2$. Phys Rev B: Condens Matter Mater Phys 72:224102–224110. https://doi.org/10.1103/PhysRevB.72.224102

[35] Julien C (2000) Structure and electrochemistry of $LiCoO_2$ from disordered to microcrystalline materials. In: Proceedings of the 3rd France-Japan Meeting on Lithium Batteries, Chamonix, May 26–27, 2000

[36] Santana IL, Moreira TFM, Lelis MFF, Freitas MBJG (2017) Photocatalytic properties of $Co_3O_4/LiCoO_2$ recycled from spent lithium-ion batteries using citric acid as leaching agent. Mater Chem Phys 190:38–44. https://doi.org/10.1016/j.matchemphys.2017.01.003

[37] Yamaki JI, Baba Y, Katayama N et al (2003) Thermal stability of electrolytes with LixCoO2 cathode or lithiated carbon anode. J Power Sour 119–121:789–793

[38] Pokle A, Ahmed S, Schweidler S et al (2020) In situ monitoring of thermally induced effects in nickel-rich layered oxide cathode materials at the atomic level. ACS Appl Mater Interfaces 12(51):57047–57054. https://doi.org/10.1021/acsami.0c16685

[39] Zou L, He Y, Liu Z et al (2020) Unlocking the passivation nature of the cathode–air interfacial reactions in lithium ion batteries. Nat Commun 11:3204–3212. https://doi.org/10.1038/s41467-020-17050-6

[40] Myung ST, Maglia F, Park KJ et al (2017) Nickel-rich layered cathode materials for automotive lithium-ıon batteries: achievements and perspectives. ACS Energy Lett 2:196–223. https://doi.org/10.1021/acsenergylett.6b00594

[41] Hwang S, Chang W, Kim SM et al (2014) Investigation of changes in the surface structure of $Li_xNi_{0.8}Co_{0.15}Al_{0.05}O_2$ cathode materials induced by the initial charge. Chem Mater 26:1084–1092. https://doi.org/10.1021/cm403332s

[42] Zhang H, May BM, Serrano-Sevillano J et al (2018) Facet-dependent rock-salt reconstruction on the surface of layered

oxide cathodes. Chem Mater 30:692–699. https://doi.org/10.1021/acs.chemmater.7b03901

[43] Aricò AS, Bruce P, Scrosati B et al (2005) Nanostructured materials for advanced energy conversion and storage devices. Nat Mater 4:366–377

[44] Mohanty D, Dahlberg K, King DM et al (2016) Modification of Ni-Rich FCG NMC and NCA cathodes by atomic layer deposition: preventing surface phase transitions for high-voltage lithium-ion batteries. Sci Rep 6:26532–26548. https://doi.org/10.1038/srep26532

[45] Zou L, Zhao W, Jia H et al (2020) The role of secondary particle structures in surface phase transitions of Ni-Rich cathodes. Chem Mater 32(7):2884–2892. https://doi.org/10.1021/acs.chemmater.9b04938

[46] Zhu J, Sharifi-Asl S, Garcia JC et al (2020) Atomic-level understanding of surface reconstruction based on $Li[Ni_xMn_yCo_{1-x-y}]O_2$ single-crystal studies. ACS Appl Energy Mater 3(5):4799–4811. https://doi.org/10.1021/acsaem.0c00411

[47] Zuo D, Tian G, Chen D et al (2015) Comparative study of Al_2O_3-coated $LiCoO_2$ electrode derived from different Al precursors: uniformity, microstructure and electrochemical properties. Electrochim Acta 178:447–457. https://doi.org/10.1016/j.electacta.2015.08.039

[48] Daxian Z (2017) Comparative study of the electrochemical behaviors for $LiCoO_2$ electrode coated with two different Al_2O_3 coating layer. Int J Electrochem Sci 12:5044–5057. https://doi.org/10.20964/2017.06.70

[49] Sheng S, Chen G, Hu B et al (2017) Al_2O_3-surface modification of $LiCoO_2$ cathode with improved cyclic performance. J Electroanal Chem 795:59–67. https://doi.org/10.1016/j.jelechem.2017.04.026

[50] Wang H (1999) TEM study of electrochemical cycling-induced damage and disorder in $LiCoO_2$ cathodes for rechargeable lithium batteries. J Electrochem Soc 146:473–480. https://doi.org/10.1149/1.1391631

[51] Wen JW, Liu HJ, Wu H, Chen CH (2007) Synthesis and electrochemical characterization of $LiCo_{1/3}Ni_{1/3}Mn_{1/3}O_2$ by radiated polymer gel method. J Mater Sci 42:7696–7701. https://doi.org/10.1007/s10853-007-1673-z

[52] Yan P, Zheng J, Zhang J-G, Wang C (2017) Atomic resolution structural and chemical imaging revealing the sequential migration of Ni Co, and Mn upon the battery cycling of layered cathode. Nano Lett 17:3946–3951. https://doi.org/10.1021/acs.nanolett.7b01546

[53] Park J-H, Cho J-H, Kim J-S et al (2012) High-voltage cell performance and thermal stability of nanoarchitectured polyimide gel polymer electrolyte-coated $LiCoO_2$ cathode materials. Electrochim Acta 86:346–351. https://doi.org/10.1016/j.electacta.2012.04.073